AD-A064 617 INDIANA UNIV AT BLOOMINGTON DEPT OF CHEMISTRY F/G 20/9
MICROWAVE-SUPPORTED DISCHARGES.(U)
JAN 79 A T ZANDER, G M HIEFTJE N00014-76-C-0838

UNCLASSIFIED NL

1 OF 1
AD
A064617

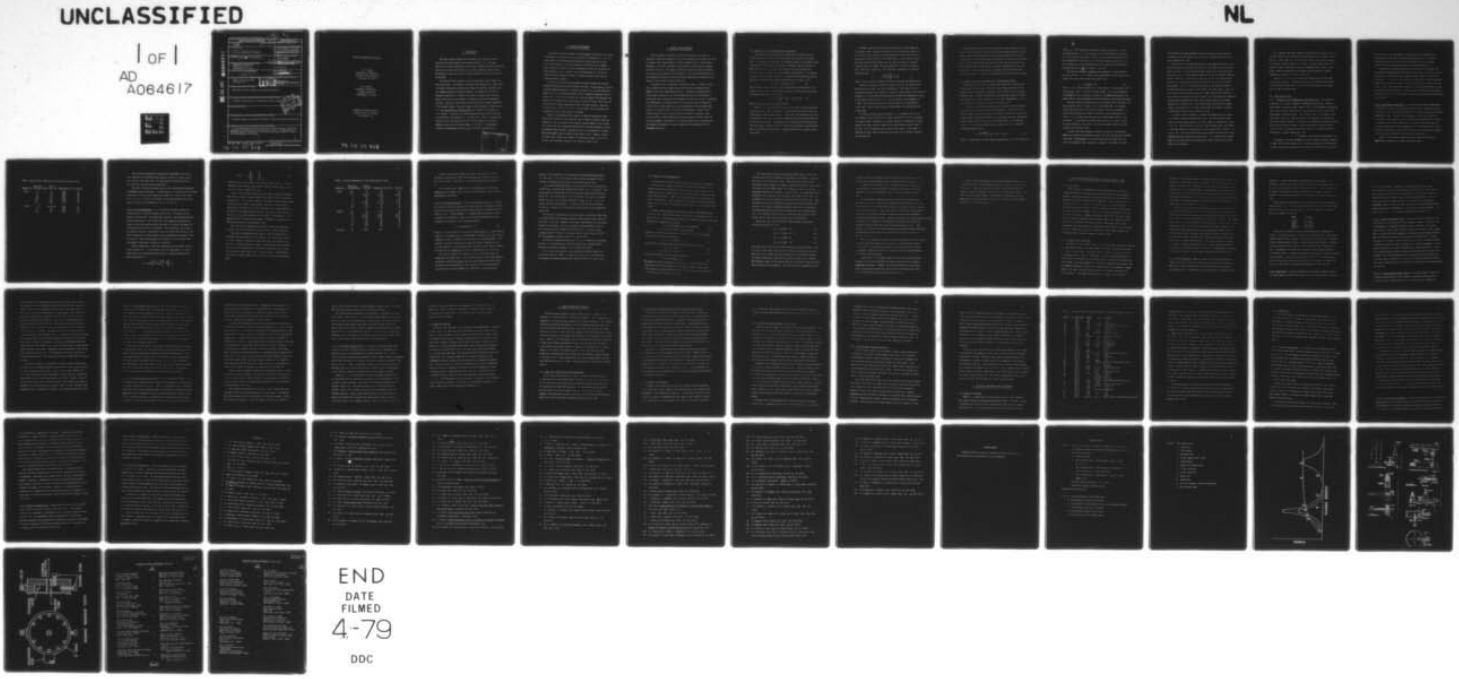

END
DATE
FILMED
4-79
DDC

AD A064617

DDC FILE COPY

SECURITY CLASSIFICATION OF THIS PAGE (When Data Entered)

REPORT DOCUMENTATION PAGE

READ INSTRUCTIONS BEFORE COMPLETING FORM

1. REPORT NUMBER: FIFTEEN

2. GOVT ACCESSION NO.

3. RECIPIENT'S CATALOG NUMBER

4. TITLE (and Subtitle): Microwave-Supported Discharges

5. TYPE OF REPORT & PERIOD COVERED: Interim Technical Report

6. PERFORMING ORG. REPORT NUMBER: 20

7. AUTHOR(s): A. T. Zander [redacted] G. M. Hieftje

8. CONTRACT OR GRANT NUMBER(s): ~~N14-76-C0838~~ N00014-76-C-0838

9. PERFORMING ORGANIZATION NAME AND ADDRESS:
Department of Chemistry
Indiana University
Bloomington, IN 47405

10. PROGRAM ELEMENT, PROJECT, TASK AREA & WORK UNIT NUMBERS: NR 051-622

11. CONTROLLING OFFICE NAME AND ADDRESS: 5.6p.

12. REPORT DATE: Jan[redacted]79

13. NUMBER OF PAGES

14. MONITORING AGENCY NAME & ADDRESS (if different from Controlling Office):
Office of Naval Research
Washington, D. C.

15. SECURITY CLASS. (of this report): Unclassified

15a. DECLASSIFICATION/DOWNGRADING SCHEDULE

16. DISTRIBUTION STATEMENT (of this Report)

Approved for public release; distribution unlimited

17. DISTRIBUTION STATEMENT (of the abstract entered in Block 20, if different from Report)

Prepared for publication in "ANALYTICAL USES OF PLASMAS"

18. SUPPLEMENTARY NOTES

19. KEY WORDS (Continue on reverse side if necessary and identify by block number)

Microwave plasmas, analytical discharges, review and emission spectroscopy

20. ABSTRACT (Continue on reverse side if necessary and identify by block number)

The fundamental operation and analytical characteristics of microwave-supported gas discharges are discussed and reviewed. The development of microwave plasma is historically traced and their future impact on analytical spectroscopy is assessed.

LEVEL

DDC FEB 14 1979 C

DD FORM 1 JAN 73 1473 EDITION OF 1 NOV 65 IS OBSOLETE S/N 0102-014-6601

UNCLASSIFIED

SECURITY CLASSIFICATION OF THIS PAGE (When Data Entered)

79 02 12 012

Microwave-Supported Discharges

A. T. Zander
Department of Chemistry
Cleveland State University
Cleveland, Oh. 44115

G. M. Hieftje
Department of Chemistry
Indiana University
Bloomington, In. 47401

prepared for publication in
"Analytical Uses of Plasmas"
R. M. Barnes, ed.

79 02 12 012

1. INTRODUCTION

Microwave-induced plasma (MIP) discharges have long been used as sources for exciting atomic and polyatomic species (1-4). The high degree of excitation afforded by such sources, coupled with their relatively low cost, have made the MIP attractive in many situations where intense, monochromatic sources are needed or where elemental emission spectra must be obtained.

The nature of MIP discharges varies considerably with the nature of their application. For example, the kind of MIP employed as a light source for atomic fluorescence spectroscopy differs considerably from that used for elemental analysis of aqueous samples. The former sort of MIP is ordinarily operated in a closed vessel and at a pressure of a few torr, whereas the latter usually employs a flowing gas system at atmospheric pressure. Logically, these different kinds of MIP are treated separately in the present volume. Enclosed plasmas used principally as light sources (i.e. the electrodeless discharge lamp) are covered in the chapter by P. N. Keliher. Similarly, gas chromatography detectors based on the MIP are discussed in the chapter by T. H. Risby and Y. Talmi. In the present chapter, we will deal exclusively with the MIP applied to the direct elemental analysis of dissolved samples. To begin, it is appropriate to place the development of such an MIP in historical perspective.

ACCESSION for
NTIS White Section
DDC Buff Section
UNANNOUNCED
JUSTIFICATION
BY
DISTRIBUTION/AVAILABILITY CODES
SPECIAL
A

2. HISTORICAL DEVELOPMENT

Excellent historical accounts of the development of the MIP can be found in the thesis by Lichte (5) and in the series by Greenfield, et. al. (6-8). Initial work in this area was performed with single-electrode plasmas (1-3, 9-20), which bore little resemblance to the devices now commonly used, and which operated at various frequencies in both the microwave and radio-frequency ranges. However, later investigations (2, 21-23) were carried out with plasmas sustained in resonant cavities, much like the currently popular systems.

It was realized early that low-power microwave plasmas are strongly affected by molecular species introduced into them. Correspondingly, initial successes employed the MIP as a detector for gases (2), for gas chromatography (21, 22), or volatilized simple, easily fragmented compounds into the plasma (23). In this latter study (23), solution samples were employed, but metals to be measured were in the form of volatile chelates, which were sent into the MIP by thermal vaporization from a platinum filament. Measured sensitivity was high (10^{-11} to 10^{-12} g. detectable), but the method could be applied to only a narrow range of elements.

Recently, investigators have sought to extend the capability of MIP analysis to elements of low volatility and to samples of greater range and complexity. These extensions have required the development of new systems for volatilizing and introducing sample material and have employed a variety of microwave power supplies, resonant cavities, and spectrometric systems. These developments will be traced in more detail later. However, because all these later systems were similar in structure and form, let us first consider the fundamental nature of the microwave plasma itself.

3. NATURE OF MIP DISCHARGES

The most commonly used and successful kind of MIP in use today is operated in inert gas (usually Ar or He) and sustained at low power (25-100W) in a quartz tube located within a coaxial resonant cavity. The microwave frequency is ordinarily 2450 MHz, chosen partially for historical reasons, but mostly because of the ready availability of low-cost medical diathermy units which provide power at that frequency. The following theoretical discussion pertains directly to this kind of MIP; additional information can be found in the excellent review by Sharp (24).

A resonant cavity, discussed in more detail later, is simply a hollow metal container having a shape and size which allow a standing electromagnetic wave to be established within it. Because the standing wave is at microwave frequencies, the cavity dimensions will be on the order of several cm; both cylindrical and rectangular cavities are in use. To generate the standing wave, microwave energy is sent into the cavity by means of a circuit loop or short, which are in turn connected to the microwave power supply via a coaxial cable. To contain the discharge, a quartz tube is ordinarily placed in the cavity along an axis which is parallel to the lines of electric field oscillation; various transverse electric (TE) and transverse magnetic (TM) modes of oscillation enable such a configuration. The formation (breakdown) of such a plasma and its maintenance will be discussed separately.

3.1. Microwave Plasma Breakdown and Stabilization

The mechanism of microwave plasma formation and stabilization are treated in detail elsewhere (24-26) and will only be briefly considered here. At extremely low pressures, an electron present in a microwave field will oscillate in position at the field's frequency, but will be out of phase with the field. Let the oscillating field E be represented by $E = E_0 \sin(\omega t + \theta)$, where E_0 is the maximum field amplitude, ω its angular frequency and θ its phase at time $t = t_0$, when the electron begins moving. The force F exerted by the field on the electron will then be (27)

$$F = ma = eE_0 \sin(\omega t + \theta) \qquad (1)$$

The resulting velocity where a is the acceleration of the electron, e its charge, and m its mass. The resulting velocity v of the electron can then be found by integration of Eq. (1):

$$v = v_0 + \frac{eE_0}{m\omega} [\cos\theta - \cos(\omega t + \theta)] \qquad (2)$$

where v_0 is the electron's initial velocity.

From Eq. (2), the electron will move as the cosine of the sinusoidally varying electric field; consequently, it will be 90° out of phase with the field and will draw no power from it. Physically, the electron is at first accelerated by the field, but cannot immediately reverse direction when the field reverses polarity. Consequently, the electron must decelerate after the field changes, and passes back to the field the energy it gained earlier. Thus, at extremely low pressures, it would be difficult to sustain a microwave plasma.

At higher pressures, the accelerating electron collides frequently with gaseous atoms, causing its direction to be altered (but largely not its velocity, since energy is exchanged between the collision partners in proportion to $2(m/M)$, where M is the atomic mass). These events continue, with the electron gaining energy from the field and losing it through collision, until it reaches an energy sufficient to excite or ionize an atom. Under these conditions, the mean power P absorbed by an electron from the field is

$$P = \left(\frac{e^2 E_0{}^2}{2m\nu}\right)\left(\frac{\nu^2}{\nu^2 + \omega^2}\right) \qquad (3)$$

where ν is the collision frequency between the electron and gaseous atoms.

From the foregoing, an optimal pressure exists for the ignition and stabilization of an MIP. At very low pressures, little power will be transferred from the field, whereas at unusually high pressures, the collision frequency is so great that an electron gains unsufficient momentum to ionize an atom upon collision (cf. Eq. 3). For the commonly used frequency of 2.45GHz, this optimal pressure has been calculated to be approximately 4 torr (29), close to those pressures found optimal in electrodeless discharge lamps.

At higher pressures (near atmospheric), it is apparent (cf. Eq. 3) that higher electric fields (E_0) or lower frequencies (ω) will be required to sustain an MIP. Ordinarily, the former approach is employed in the MIP whereas the latter factor is exploited in radiofrequency plasmas such as the ICP. For an atmospheric-pressure MIP, power inputs in the range of 100W are utilized, while a lower pressure plasma can be readily sustained at less than 25W.

Stabilization of the MIP arises essentially through repetition of the processes outlines above. Successive collision between electrons released through ionization and remaining neutral gas atoms progressively ionizes a greater fraction of the gas, until the energy contributed by the microwave field is partitioned between the moving electrons and the generated ions. Significantly, little of this energy is directly contributed to the ions by the field; their considerable mass prevents them from gaining much translational energy in the brief period before the field reverses polarity.

3.2. Energy Coupling to and Stability of the Microwave Plasma

Maintenance of an MIP can be understood through the following model of the plasma-cavity system. From this model, plasma and power balance equations can be formulated, assuming a cavity resonance near the plasma frequency (30). Although the model does not take into account the radial electron profile and the consequent electric field inhomogeneity, it has proven useful for a number of RF plasma systems (31-33).

A steady-state microwave discharge occurs when the power absorbed by the plasma equals the power losses from the plasma. Such losses occur mainly through inelastic collisions resulting in excitation or ionization, through energy transported to the walls by electrons and ions, and through energy transported out of the active discharge region in a flowing gas system. For a particular plasma geometry, power loss P_l is a function of average plasma density:

$$P_l = \left(\rho^2 \frac{mE_0}{e}\right) (\nu_i V_i + \beta T_e + \Sigma\nu_x V_x) \qquad (4)$$

where ρ is proportional to the average plasma density, V_i is the ionization

energy, ν_i is the frequency of ionization-causing collisions, V_x is the excitation energy, ν_x is the frequency of excitation-producing collisions, T_e is the electron temperature, and βT_e is a term which represents energy loss transported to the walls by the electrons and by the ions (30). A plot of power loss versus plasma density for a constant gas pressure has continual positive slope (cf. Figure 1, curve A).

The time-averaged power absorbed by the plasma P_a is found from the real part of the complex Poynting vector integrated over the surface of the plasma (the average ohmic power dissipation) (34):

$$P_a = (1/2)R_e\int_V \sigma E^2 dV \qquad (5)$$

where σ is the complex conductivity of the plasma, E is the electric field in the plasma, and V is the entire plasma volume. For a given impressed electromagnetic field strength P_a depends on the damping mechanism of the plasma and the coupling between the fields external to and within the plasma.

From the foregoing considerations and an assumed cavity structure, the power-absorbed curves in Figure 1 can be calculated (30). At constant incident microwave power, excitation frequency, and cavity dimensions, a single power-absorbed curve would be observed as the plasma density is varied. (It is assumed that the absorbed microwave power does not alter the plasma.) Increasing the incident power from $P_a(1)$ to $P_a(2)$ raises the power absorbed by the plasma, since field strength inside the cavity increases with incident power.

A steady-state high-frequency discharge can only be sustained when there is an intersection between the power loss curve and the power absorbed curve (30). Understandably, at intersections where the power absorbed curve has a negative slope, stability is implied. Conversely, at inter-

sections where the power absorbed curve has a positive slope instability is implied, unless the power loss curve slope is greater than that of the power absorbed curve (30).

Curves B and C illustrate the behavior of the stable plasma and cavity when the excitation frequency and cavity size are fixed, but the microwave power is varied. A stable operating point (point 4) at a particular incident power $P_a(1)$ is established primarily by the cavity resonant frequency. However, when the incident power is raised to $P_a(2)$, the plasma density increases, the operating point moves to point 5, and the cavity becomes more detuned. That is, only a small fraction of the additional power is absorbed and the excess power is reflected to the power supply. Thus, the very increase in plasma density which is sought prevents much additional power from being introduced into the plasma. Even the addition of impedance matching devices between the cavity and the power supply only slightly improves this situation (35). This small change in density for a large change in incident power is a major problem when one attempts to produce a high density plasma inside a microwave cavity.

A solution to this problem is to adjust the dimensions of the cavity. At a constant incident microwave power level, the power-absorbed curve shifts to higher plasma densities as cavity length is increased (cf. curve D, Fig. 1). Note from curve D that at a fixed incident power, the height of the power-absorbed curve decreases as the plasma density increases. At point 6, the intersection between the power-absorbed and power-loss curves indicates marginal stability for the plasma. For a greater cavity length than L_2, the plasma would be extinguished, and the plasma-cavity system drops out of resonance.

It is apparent from these arguments that ignition and stable operation of an MIP should be most efficient at two different cavity lengths. Before ignition, plasma density is low (essentially zero), and reliable ignition will require a shorter cavity (cf. curve B). However, plasma density will rapidly increase after ignition and with increased power (curve C), and stable, efficient operation of the higher-density plasma will require lengthening (retuning) the cavity (curve D).

The curves of Figure 1 are plotted for constant pressure and fixed cavity input coupling. Altering the pressure will change both the power-loss and power-absorbed curves; altering the input coupling will change only the power absorbed curves.

3.3. MIP Characteristics

3.3.1. *Plasmas in Local Thermodynamic Equilibrium (LTE)*. No laboratory plasmas are in a state of complete thermodynamic equilibrium. However, in some plasmas, individual volume elements obey all thermodynamic distribution laws, except Planck's radiation law; such plasmas are said to be in local thermodynamic equilibrium (LTE). The concept of LTE is very useful, since under such conditions, energy and volocity distributions are governed by Maxwell-Boltzmann relations. Furthermore, the Saha-Eggert law then describes the yield of ionization products, and the population of discrete energy levels follows a Boltzmann distribution. That is, a plasma in LTE can be described by a single temperature T, and

$$T = T(\text{kinetic}) = T(\text{reaction}) = T(\text{excitation}) \quad (6)$$

In plasmas at or near atmospheric pressure, where the particle density is high, LTE is often attained (27). A Boltzmann expression will determine specific energy level populations, the fraction of ionized species present

will be given by the Saha equation, and the state of the plasma will be characterized by the measured temperature and density (27). For such plasmas there need be less concern for the details of the microscopic processes which constitute the plasma excitation mechanisms (36).

For plasmas at reduced pressure, particle density is decreased, and each particle undergoes fewer collisions per unit time. In turn, collisions are necessary to partition energy among the various states the particles can possess. As a result, such plasmas are seldom in LTE, and an inordinate amount of their energy is stored in electron motion or in excited electronic states. These states then radiate energy at a level unexpected for a plasma at that particular power input. In such a case, the microscopic excitation mechanisms would have to be detailed for optimum utilization and understanding of the plasma.

3.3.2. Spectroscopic Temperatures. The electronic excitation temperature of a microwave plasma can be derived from the relative radiances of inert gas spectral lines having known wavelengths (λ), energy levels and transition probabilities (A_{ki}). A plot of log ($B\lambda/g_k A_{ki}$) vs. log (E_k) (where B is the spectral line radiance, g_k is the statistical weight and E_k the energy of the upper state of the transition), will yield a line whose slope is inversely proportional to the temperature (37). The largest error in such temperature measurements arises from uncertainty in the transition probabilities (A_{ki}) which are known only to within about 20% (38).

Table 1 lists excitation temperatures for argon and helium MIP's under varied conditions of pressure and applied power.

TABLE 1 Spectroscopic Temperatures of Microwave-Induced Plasmas

Support Gas	Operating Pressure (Torr)	Applied Power (W)	Temperature (°K)	Reference
Argon	3	25	4150	36
	12	25	4285	36
	12	100	4060	39
	25	25	4535	36
	630	100	4850	39
	760	100	4980	40
	760	100	5100	41
Helium	1.07	not given	2300	42
	2	50	8550	43
	5	80	3350	39
	760	100	7250	44

The excitation temperatures obtained from measurements of inert gas line intensities are dependent upon pressure, but not to a great extent. At a constant input power level the spectroscopic temperature increases at a very slow rate with inert gas pressure.

The effect of applied microwave power on the spectroscopic temperature is dependent upon the pressure. At high pressures, an increase in the applied power tends to decrease the temperature slightly or to have little effect at all. At lower pressures, an increase in the applied power causes only small elevations in the temperature (36, 42, 43, 45, 46).

3.3.3. Electron Temperature. In a low-pressure microwave plasma, two distinct groups of electrons appear to exist (36). One group, at low density (concentration), has high energy (velocity) and dominates measured electron temperatures. As we shall see, this temperature describes the energy of these high-speed electrons and serves to indicate the degree of excitation and ionization in the plasma. The second group, consisting of low-velocity electrons, constitutes by far the largest fraction and is the prime contributor to electron number density measurements discussed in the next section. Because both groups are significant, let us examine these measurements (temperature and density) separately.

Electron temperature is most often measured using the double electric probe technique (47). In this method, electron temperature, T_e, can be found from a plot of measured probe current vs. applied potential (the probe characteristic):

$$Te = 11600 \left[\frac{X}{(1 + x)^2}\right] \left[\Sigma i_1 \frac{dV}{di}\right]_{v=o} \qquad (7)$$

where $$\chi = \left[\frac{\Sigma i_i}{i_{e1}} - 1\right]_{V=o} \qquad (8)$$

and where dV/di is the slope of the current-voltage curve, Σi_i is the summation of the positive ion currents evaluated at V=0, and i_{e1} is the electron current to probe 1 (36, 48).

Table 2 lists electron temperatures for argon, helium and nitrogen MIP's under a number of applied power and operating pressure conditions, obtained by the double probe technique. The highest electron temperatures are obtained for helium. Interestingly, the ratio of the excitation temperatures obtained in He to those obtained in Ar is approximately 1.6 at any particular power-pressure setting. This value is very close to the ratio of ionization potentials for the gases: IP(He)/IP(Ar) = 1.57, suggesting that the mean electron energy is primarily a function of the ionization potential of the plasma gas (36).

Note that electron temperatures decrease as the plasma pressure is increased. At gas pressures above about 4 Torr T_e remains constant.

The effect of applied microwave power on electron temperature is dependent upon the pressure of the inert gas. At low pressures (below $\sim$ 5 Torr), changes in applied microwave power have little effect on T_e (36, 43). At higher pressures, changes in applied power have a greater effect on electron temperature, although the temperature will be lower for any specific power input than at a lower pressure. Understandably, an increase in applied power causes an increase in the electron temperature.

TABLE 2 Electron Temperatures of Microwave-Induced Plasmas

Support Gas	Operating Pressure(Torr)	Applied Power(W)	Temperature $X10^{-3}$(°K)	Reference
Argon	0.1	50	45	50
	0.5	50	30	50
	1	50-120	26-53	43,47
	2	120	38.3	47
	3	25	35	36
	4	120	35	47
	6	25-120	34.2-35	36,47
	8	120	33	47
	10	120	35	47
	12	25	35	36
Helium	0.1	50	130	50
	0.5	50	75	50
	1	50-120	63-90	43,47
	2	50-120	63-75	43,47
	3	25	50	36
	4	120	55	47
	6	120	50	47
	8	120	50	47
	10	120	50	47
Nitrogen	760	1000	∿100	1

A greater flow rate of support gas causes a decrease in T_e (49). The effect is greatest at lower flow rates and tends to decrease as the flow rate increases. The effect is also more pronounced for He than for Ar.

It is evident from a comparison of the spectroscopic and electron temperatures (cf. Tables 1 and 2) that a low pressure MIP is not in local thermodynamic equilibrium.

3.3.4. Electron Concentration. The electron number density, n_e, in microwave plasmas reflects principally the concentration of low-energy electrons and can be obtained from the current-voltage behavior of double electrical probes (1, 51). In that method, it is assumed that the positive ion concentration in the plasma is equal to the electron concentration, so the saturation ion current I_+ to an individual probe is:

$$I_+ = 0.6\ n_+ eA(kTe/m_+)^{1/2} \qquad (9)$$

where n_+ is the positive ion (or electron) number density, e is the electron charge, A is the probe area, k is Boltzmann's constant, T_e is the electron temperature, and m_+ is the mass of the positive ions being detected. This equation is strictly valid only for spherical probes in plasmas at low pressure; however, it has been used with cylindrical probes and at elevated pressures for the estimation of electron concentrations (1, 36, 48, 49).

The electron density in a plasma can also be calculated from line broadening measurements (43). The electrons present in the plasma generate an electric field which broadens spectral lines through the Stark effect; the extent of such broadening is then a measure of the electron density. Spectral lines of atomic hydrogen are often used in such measurements

because of the availability of tabulations of Stark boradening parameters for those lines. Also, the theory is more accurate and somewhat simpler to apply to hydrogen than to multielectron atomic species (38).

In a typical Stark measurement, the line profile of the H_β transition at 486.13 nm is measured and the Stark half-width, $\Delta\lambda_s$, is estimated. From these values and tabulations (43) of the proportionality factor between n_e and $\Delta\lambda_s^{3/2}$, the electron density can be estimated. The H_β-line is chosen because the range of half-widths expected is large (ca. 1.0 - 5.0A°) for typical electron concentrations. In addition, the relationship between $\Delta\lambda s$ and n_e is known for this line over a broad range of n_e and temperature values (38).

The electron concentration in an argon plasma is generally higher than in a helium MIP at all operating pressures, applied power levels, and flow rates (36, 43, 48, 49). However, the electron concentration for both gases increases with pressure, the rate of change decreasing between 2 and 10 torr, above which little effect of pressure occurs. For such plasmas, n_e ranges from 10^{11}-10^{12}cm^{-3} at pressures below 1 torr to about 10^{15}-10^{16} cm^{-3} at atmospheric pressure (36, 38, 41, 45, 48, 49).

The effect of applied microwave power on n_e is influenced by operating pressure. At low pressures n_e increases rapidly with increased power, whereas the increase with power is less at higher pressures.

The electron concentration is only moderately affected by gas flow rate at any pressure. There is a gradual increase in n_e as the flow rate is increased, but beyond approximately 200mL/min there is no effect (49).

3.4. Analyte Excitation Mechanisms

A discussion of the processes by which analyte spectra are produced by an inert-gas MIP requires knowledge of the nature and energies of the atomic and molecular species which can be present in the plasma, the excitation processes in which they can be involved, and the analyte atom and ion excitation energies. Both ion and neutral atom line emission are produced. Unfortunately, complete support for any single excitation mechanism seems not to exist and the following coverage provides an overview of likely events.

In both low and high-pressure microwave plasmas, high and low energy electrons, ions, and metastable atoms and molecules are present (36, 43, 49, 50, 52-55). The low-energy electrons are in abundance and are especially effective in recombination excitation:

$$e + G + M^{+} \longrightarrow G + M^{*} + h\nu(\text{continuum}) \qquad (10)$$

$$\text{or } e + G^{+} \longrightarrow G^{*} + h\nu(\text{continuum}) \qquad (11)$$

where G is an inert gas atom and M is an analyte atom. The high energy, fast electrons sustain the plasma by:

$$e + G \longrightarrow G^{+} + 2e \qquad (12)$$

but can also be involved in direct excitation processes such as:

$$e + M \longrightarrow M^{*} + e \qquad (13)$$

$$\text{or } e + M^{+} \longrightarrow M^{+*} + e \qquad (14)$$

Ions can be involved in the excitation process by:

$$G^{+} + M \longrightarrow G + M^{+*} \qquad (15)$$

The condition for the occurrence of reaction 15 is that the sum of the ionization and excitation energies of the analyte atom be almost equal to the support gas ionization energy (52). The ionization energy of argon is 15.76eV and that of Helium is 24.59eV.

The inert gases all possess metastable levels (atoms in the lowest triplet state) which also appear to participate in excitation. Argon has two levels, at 19.73eV and 20.53eV. Inert gas atoms can reach these metastable states through, for example, excitation followed by collisional de-excitation with another ground state support gas atom (53) or from sequential occurrence of reactions 12 and 11 above. The population of the metastable levels decreases with pressure, up to about 20 torr (36, 53), presumably because of increased two-and three-body collisions (56). Above approximately 20 torr the metastable population increases regularly with pressure. An increase in applied microwave power causes an increase in the metastable population, but the increase tapers off at higher powers (36). The lifetime of these levels is relatively long since only collisional, and not radiational, deactivation occurs appreciably.

Metastables (G_m) can be involved in the following ionization or excitation processes (52, 53):

$$G_m + M \longrightarrow G + M^+ + e \tag{16}$$

$$G_m + M^+ \longrightarrow G + M^{++} + e \tag{17}$$

$$G_m + M \longrightarrow G + M^* \tag{18}$$

$$G_m + M^+ \longrightarrow G + M^{+*} \tag{19}$$

Reactions 16 and 17 are the well-known Penning ionization processes. They can occur if the energy of the particles before the collision is greater than the first or second ionization energy of M; the difference between the energy of metastable atom and the ionization energy of M is carried off as kinetic energy of the ejected electron. Reactions 18 and 19 involve direct excitation by metastables. They are relatively improbable and can

occur only under the rigorous condition that the excitation energy of the analyte atom be approximately equal to the metastable energy (52).

In addition to metastable atoms, metastable molecules and molecular ions are known in inert gas plasmas and might be involved in excitation processes (52, 53); these molecules have a range of energies available (52).

It is now widely accepted that direct excitation of analyte atoms and ions by electron collision is not dominant in an MIP (36, 49, 52, 53). Fewer lines are observed than expected from the continuous range of energies available with electrons. Also, the features of the spectra do not change with pressure as would be expected, considering the pressure dependence of electron temperature (52, 53). Instead, the dominant excitation process has been interpreted as a sequence of steps beginning with impact by metastables leading to Penning ionization of the analyte (reaction 16 or 17). This process is followed by ion recombination with low-energy electrons producing excited analyte atoms, which then radiatively deactivate (reaction 11) (36, 49, 52, 53).

From this mechanism, an increase in pressure should lead to an increase in analyte emission, because of the greater metastable population above about 20 torr. An increase in pressure will also decrease the electron temperature, leading to an increase in analyte emission through promotion of electron-ion recombination.

A small increase in microwave power, for both low and high pressure plasmas, will lead to an increase in analyte emission due to a greater metastable population. However, this increased emission is not without limit, because higher power will increase electron concentrations which will in turn promote collisional deactivation (10).

If one accepts the foregoing ionization-recombination model, it is clear why the MIP is such a promising analytical source. A brief glance at a table of elemental excitation energies (57-59) reveals that most elements would be efficiently excited by Ar or He metastable atoms. Not only would "difficult" elements like nonmetals or halogens be excited, but neutral atom and ion lines would often be available, thereby adding flexibility to a determination.

4. INSTRUMENTATION FOR PRODUCTION OF MICROWAVE-INDUCED PLASMAS

4.1. Power Units

Early versions of instrumentation for the production of microwave-induced discharges were fashioned from government-surplus radar equipment. Clearly, significant microwave engineering knowledge would be required to assemble an adequate system from such components. Later, the need for less expensive and artificial sources of continuous-wave (cw) microwave power was fulfilled through the use of medical diathermy units which supply about 125-200W peak power at 2450MHz. Today, the increasing popularity of microwave ovens operating at 2450MHz has markedly reduced the cost and increased the availability of magnetron power sources; however, the commercial availability of cw microwave power units with the power range, stability and operational character needed for spectroscopic applications is still severely limited. Information on specific commercial microwave power supplies can be found in many electronics components buyer's guides.

4.2. Resonant Cavity Structures

The purpose of the resonant cavity is to transfer power efficiently from the microwave power source to the inert support gas, which is generally contained in a glass or quartz tube. A resonant cavity structure is used to increase the electric field in the gas. Ordinarily, some sort of coupling device is used to match the impedance of the resonant cavity to that of the transmission line leading to the power supply (60). When these impedances are matched, and the resonant frequency of the cavity is tuned to that of the magnetron (power supply), the power reflected from the cavity is a minimum; conversely, the power available to the plasma will then be at a maximum. The attainable

minimum value of reflected power is dependent upon the type of cavity used and on its construction; the most efficient cavities will be those with the highest "Q-factor" (33). Unfortunately, the presence of a plasma in the cavity changes its resonant frequency, thereby detuning it and reducing the Q factor (33). Because the character of the plasma changes with pressure, power input and gas type, it is necessary to provide the cavity with tuning and impedance-matching adjustments to obtain efficient operation over a wide range of discharge conditions (33, 61).

A detailed discussion of the operating modes of microwave cavities for plasma production would necessitate a thorough review of microwave transmission line theory and its extension to cylindrical resonators of specific cross-section, an endeavor far beyond the scope of this chapter. The interested reader is referred instead to literature sources (34, 62–64). In the following sections, we will describe several of the more frequently used cavities and their modifications. The resonant modes of some of these cavities cannot always be separated into purely transverse electric (TE) or transverse magnetic (TM) modes; most modes have both TE and TM contributions and are called "hydrid" modes. The cavity structures are often too complex to analyze electromagnetically, and the exact mode character is not known or definable for many of them (33). Designations of the basic cavities used below were coined by Ramo, Whinnery, and Van Duzer (62).

4.2.1. Cavity Materials. Maxwell's equations for wave propogation in resonant microwave cavities show that the fields and currents produced in the cavity decrease exponentially with penetration into the conductive cavity material (62). The degree of this penetration is indicated by the

parameter δ (called the "depth of penetration" or "skin depth" of the material), defined as the depth at which the field or current has decreased to 1/e of the respective value at the material surface. The skin depth will be smaller for material of higher conductivity or at higher frequencies, because it is inversely proportional to the square root of these quantities (34).

The operational significance of the skin depth resides in the amount of applied power which is lost as thermal heating of the cavity and in the maximization of the cavity quality factor, Q. The skin depth for a number of metals at 2450MHz is given (65):

METAL	δ (cm)
Silver	1.3×10^{-4}
Copper	1.3×10^{-4}
Gold	1.6×10^{-4}
Aluminum	1.6×10^{-4}
Brass	2.7×10^{-4}

The choice of material for the cavity depends upon a compromise of factors. For highest cavity Q, very pure silver would be best, with copper second, and gold third. However, these pure metals are difficult to machine and the resulting cavity surface is always marred, which reduces Q; moreover, Cu and Ag surfaces corrode rapidly in air and become less conductive with time. Consequently, the ideal cavity materials do not allow construction of the best cavities. Construction from brass followed by a 2μm-thick plating with Ag affords a cavity with a sufficiently high Q. The Ag-coated brass cavity can be given a thin film coating of Au, by flashing, to protect the Ag finish; the cavity Q is essentially unaffected by this last step.

4.2.2 Cavity Types. The most frequently used microwave resonant cavities for spectrochemical studies have been described in various degrees of detail

(2, 33, 45, 61, 66-68). Descriptions of modifications to these basic cavity types (39, 69-72), of a new-design cavity (42, 52, 73, 74), and of less well-used versions (75-77) have appeared. The principal features and operating character of these cavities will be described below. The basic cavity types (61) are shown in Figure 2. The cavities are designed to accommodate glass or quartz discharge tubes and can be modified, generally without impairment of performance, to accept tubes of varying diameter. The tube is always located in a region of strong electric field (61).

4.2.2.1. Tapered Rectangular, TE_{013}. The cavity shown in Figure 2a is one of the earliest cavities used for spectrochemical studies. It consists of a low-impedance, rectangular waveguide which is connected to an E-plane taper section at one end and is short-circuited at the other. The discharge tube is inserted into this waveguide at a quarter-guide wavelength distance from the short-circuited end, in the electric field direction. A useful feature of this design is that the cavity can be placed in position without disturbing the quartz or glass discharge tube; such an arrangement is particularly convenient is the tube is attached to a vacuum system (61). A screw in the coupling probe permits adjustment of the probe depth to achieve best coupling. The resulting plasma exists principally within the confines of the cavity edges, resulting in a short, well-located discharge for viewing. This cavity operates best at low pressures of support gas, below approximately 50 torr (61).

4.2.2.2. Foreshortened 3/4-wave Coaxial. The cavity shown in Figure 2b is a coaxial resonator made of two concentric conducting cylinders with a gap in the inner cylinder which acts as a capacitive line termination.

The discharge tube is inserted through the center of the inner cylinders. Tuning the cavity is accomplished by varying the gap distance between the inner cylinders with the threaded inner cylinder. One modification of this cavity, for use entirely within a vacuum apparatus, has replaced the screw type cylinder with a sliding sleeve (69). The width of the gap is always such that the inner cylinder of the cavity is a waveguide beyond cutoff at 2450 MHz so that the cavity effectively confines the microwave radiation. The hose-fitting on the coaxial connector is for a cooling air flow to prevent overheating. The plasma exists in the discharge tube in the gap between the inner cylinders and is essentially the length of the gap. Small carbon washers within the plasma chamber to one side of the gap have been used to stabilize the location of the plasma in discharge tubes much larger than the plasma diameter (41). The hole in the outer cylinder allows radial viewing of the plasma. Atmospheric pressure operation of the plasma allows axial viewing (66, 67). A disadvantage of this type of cavity is that positioning of the cavity requires breaking the vacuum line for vacuum operation.

The cavity in Figure 2c is identical to that in Figure 2b except for the addition of an adjustable matching stub located on the coaxial connector. This stub simplifies cavity tuning. These cavities, which operate most efficiently from about 1 torr to atmospheric pressure (45, 61), have become known collectively as the 3/4-wave Broida cavity (45). Another version of the 3/4-wave coaxial cavity in which the gap is held constant and tuning is performed with a matching stub or coupling slider, or both, and whose outer conductor radius is increased, is known as the 3/4-wave Evenson cavity (45).

4.2.2.3. Foreshortened 1/4-wave Coaxial. The cavity shown in Figure 2d is also a coaxial resonator, but is constructed such that the gap is fixed and the discharge tube runs transverse to the gap. Tuning is accomplished by means of a stub on the body of the cavity and a slider on the coaxial coupling (61); correct tuning requires successive readjustment of each. The removable end cap allows the unit to be positioned without breaking a vacuum system (61) and is one of the principal reasons the cavity has been extensively used. The plasma is usually viewed radially through a hole or slit in the end cap. These cavities operate well from low to moderate pressures (45, 61), and it has been found that the discharge can be stabilized by surrounding the cavity with a magnetic field (72).

One version of this cavity has the tuning stub positioned along the axis of the discharge tube (70), since adjustment of the power coupling has been shown to lead to more than one condition of minimum reflected power. But the plasma discharge is stable at only one setting, and also arcing between the coupling probe and tuning stub can occur (61, 71). This disadvantage has been minimized with the addition of side extensions, along the discharge tube axis, on the body of the cavity and the end cap (71). The discharge exists in the gap and is approximately confined by the cavity body.

4.2.2.4. Foreshortened 1/4-wave Radial. The cavity shown in Figure 2e is a resonant radial transmission line loaded or foreshortened by the capacitance of the gap or tuning post (61, 62). Tuning is accomplished with a centrally positioned screw. Power coupling results from making the coupling loop large enough to ensure perpendicular intersection with the magnetic fields of the cavity. Cavity cooling air is introduced with a connection on the coaxial connector. Location of the discharge tube on early versions of this cavity

was optimized by trial and error (61). Although the cavity operates well over a wide range of pressures, it is most efficient at low pressure; at higher pressures the discharge is confined to a region close to the discharge tube wall nearest the coupling loop, resulting in spot heating of the tube. Ordinarily, the plasma is viewed axially.

A significant improvement in the design characteristics and operation of this type of cavity has been reported by Beenakker (52, 73, 74). The new cavity was designed specifically for operation at atmospheric pressure with either argon or helium. Principal considerations taken into account during design were: a) having the resonance frequency at exactly 2450 MHz; b) minimal cavity volume so a high energy density could be attained; c) location of the discharge at the position where the electric field is greatest. To meet these needs, Beenakker devised a structure to operate in the TM_{mn0} modes, in which the resonance frequency is independent of the height of the cavity (73). The electric field can then be increased simply by decreasing the cavity height without upsetting resonance conditions. The smallest cavity diameter and hence the largest energy density is obtained when m=0 and n=1; for 2450 MHz the diameter is calculated to be 93.7mm (73).

Figure 3 shows a schematic diagram of this TM_{010} mode cavity. Because the electric field is maximal in the center of the cavity, the discharge tube is located axially in that location. Microwave power is transferred to the cavity by means of a coupling loop perpendicular to the circularly directed magnetic field (73).

The introduction of dielectrics, such as a quartz plasma tube, into the cavity shifts the resonance frequency to lower values. Consequently, the cavity diameter must be calculated for a resonance frequency slightly above the input frequency. Thus, the diameter of the cavity should be

chosen slightly smaller than calculated without a plasma present. The tuning stub can then be used to adjust for the resonance condition.

The plasma produced in helium is self-igniting at atmospheric pressure and is highly stable (44, 73). It exists within the boundaries of the cavity, about 1 cm long, and is viewed axially. Interestingly, the optimal location for an argon plasma tube has been found to be near the outer rim of the cavity, rather than centered, unless an impedance matching device is inserted between the cavity and transmission line (74). For He or Ar, a significant advantage is that the plasma is physically situated close to the edge of the cavity, simplifying interfacing with sample injection systems.

4.2.2.5. Waveguide-coupling Cavities. In general, microwave power transmission will be more efficient when the transmission line components have dimensions close to the wavelength of microwave radiation (34, 62, 65). For this reason, microwave torch discharges, which consume an order of magnitude greater power than MIP's, are usually capacitively coupled to waveguide transmission lines (7). MIP's in waveguide cavities or with cavities coupled to waveguide lines (75-77) have been reported. However, the use of waveguides in this fashion is much less frequent than coaxial-component systems.

Hattori, et al. (75) described a coaxial open-ended resonant cavity for the production of a long plasma discharge in Xe at low pressures. The cylindrical cavity resonator is matched to a rectangular waveguide with a doorknob antenna (75). The plasma consumes up to 1 KW and operates at 2450 MHz. Bovey (76) described a tunable microwave waveguide cavity for 2450 MHz operation. Tuning sliders and adjustable-screw short-circuits enable fine tuning of the capacitively coupled plasma, which is used as a light source rather than a sample excitation source. De Corpo, et al. (77)

described a waveguide into which a discharge tube is mounted off-axis for inductively coupling low levels (<200 mW) of 2450 MH microwave radiation to flowing inert support gases. The system is used to generate atomic species for plasma studies.

4.3. Radiation Exposure

Microwave stray radiation can be injurious to the experimenter, especially to parts of the body where heat cannot be carried away efficiently, such as the eye. Safety standards in most countries are based on the heating effects of microwave radiation and are 10mW/cm^2; whereas the U.S.S.R. has set a more restrictive continuous exposure level, based on biological studies, of 0.01 mW/cm^2 (77). Reports dealing with microwave stray fields and the influence of carrier gas pressure and type (72, 77) and cavity design and shielding (78, 79) have been published. The distribution of the microwave stray field around an MIP set at optimal conditions in a normal laboratory will be inhomogenous because of reflection and absorption by surrounding components (79). Stray radiation will increase by approximately an order of magnitude when the carrier gas pressure is decreased an order of magnitude, or when the applied power is increased from 50 to 175W (79). Power densities of 2 to 35 mW/cm^2 within 1 meter of typical MIP components have been measured (77 - 79) and demand some sort of shielding. Fortunately, stray radiation can be effectively reduced to safe levels by enclosing the apparatus in a simple aluminum box or with aluminum-foil wrapping (79).

5. SAMPLE INTRODUCTION TECHNIQUES

Microwave-induced plasmas in argon or helium possess a number of advantages as excitation sources in emission spectrometry. The plasma excitation temperatures are generally high enough that a significant number of the elements, including the halogens and nonmetals, can be determined with high sensitivity in the ultraviolet and visible regions. Also, the power required for stable operation of an MIP is relatively low, generally below 200W, making the systems relatively inexpensive and reducing the influence of radiofrequency interference noise. However, this same feature causes a difficulty when an MIP is interfaced to some type of sample introduction system. The low power does not afford a high enough plasma energy density to vaporize or evaporate solid or liquid samples, or to atomize the analyte species. Also, the stability of the plasma can be degraded when even a relatively small amount of sample material is injected into it. These problems have not proven insurmountable, but they have hindered extensive use of MIPs in optical emission analysis for solution samples.

5.1. Vapor Phase Introduction-Gas Chromatography

By far, the most extensive use of MIPs as emission sources has been in combination with gas chromatographic systems (21, 22, 42, 52, 73, 79-101). The GC carrier gas can be argon or helium and the generally used flow rates are compatible with stable MIP operation. In such an application, the MIP has been employed to excite elements such as C, H, N, P, B, O, and the halogens, providing highly selective and sensitive detection and determination. Chapter 00 of this text gives an extensive coverage of this topic.

5.2. Vapor Phase Introduction-Generation of Gaseous Analyte Species

Vapor-phase injection of the sample into the MIP can be accomplished through the direct injection of a gaseous sample (102) or through production of a gaseous compound of the analyte. A generator for the production of gaseous hydrides could be utilized in this manner. Appropriate insertion of the generator into the support gas manifold (103) or some sort of valving system which allows sequential hydride production/generator flushing would afford simple interfacing. Similarly, gaseous mercury production chambers can be inserted into the inert gas lines for simplified Hg determinations (104, 105). A generator for the production of gaseous chlorides of Bi, Cd, Ge, Mo, Pb, Sn, Tl, and Zn has also been reported (106).

The principal interfacing problem encountered with gaseous generators is maintenance of a stable support gas flow to the MIP. Sample injection into an on-line port, or valve switching for generator flushing can introduce a discontinuity in the support gas flow which is manifested as erratic background emission. Of course, this problem is not present if the species to be determined are present in the support gas itself. Such an approach has been employed for the determination of C, H, O, and N-containing contaminants in high-purity argon (107).

5.3. Sealed-cell Excitation

Extremely high sensitivities for several elements have been obtained by sealing samples of the elements into evacuated quartz cells and exciting the metals in a microwave field (108-111). In the method, solutions of the metals (as iodides) are prepared and small amounts (50μL) added to a quartz cell. Addition of excitation buffers (Bi iodide) and suitable scavengers

(Ge), followed by freeze-drying and excitation in a hydrogen atmosphere (5 torr) provides sub-picogram detection limits for Cd, In, Tl, Zn, Te and Se.

5.4. Solution Introduction-Nebulization Systems

Spraying solution samples into an MIP presents difficult problems. The low energy density and low kinetic temperature of a typical MIP do not provide efficient evaporation and atomization of the sample droplets. In helium MIPs the problem is exacerbated since most pneumatic nebulizers will not operate with helium at the support gas flow rates (20-700mL/min) required for stable MIP operation. However, pneumatic nebulization into argon MIP's can be accomplished if an aerosol desolvation system is located after the nebulization chamber (40, 45, 66). With such an arrangement, aqueous nebulization rates of 1.1-1.5mL/min have been attained. Removal of much of the aqueous solvent minimizes the evaporation requirement of the plasma.

Beenakker (73) circumvented the nebulization problem for helium plasmas by utilizing a special low-flow nebulizer (112). With this nebulizer and a new kind of MIP cavity, he was able to sustain an atmospheric-pressure helium MIP with injection of 1.7mL/min aqueous sample (5% nebulizer efficiency gave approximately 85mg/min water injection) without desolvation. Unfortunately, the presence of larger droplets upset the signal stability. Aqueous sample nebulization can also be accomplished using ultrasonic nebulization (113). Kawaguchi, et al. (113) report aqueous nebulization rates of approximately 0.5mL/min with an ultrasonic nebulizer followed by a desolvation system.

No matter how closely-matched to MIP flow-rate and particle loading characteristics a pneumatic or ultrasonic nebulizer might be, and regardless

of whether the aerosol is desolvated, the foregoing devices still require the MIP to atomize an injected analyte. Such an approach, in our view, will never gain widespread acceptance for low-power MIP devices. Rather, it would seem that analyte should be pre-atomized or pre-vaporized before insertion into the discharge, allowing the MIP to perform the task for which it is best suited--excitation. Of course, an alternative approach is to increase the applied power to the plasma sufficiently to permit atomization or acceptance of larger sample injection rates; this concept has been employed in the design of so-called microwave torches (114-116). Unfortunately, such devices lose the low-power advantage of the MIP.

5.5. Electrothermal Sample Introduction

Electrothermal atomization constitutes a nearly optimal technique for introduction of solution or solid samples into an MIP. All versions of electrothermal atomizers (ETAs) can operate in inert gas environments and can be readily inserted into the MIP support-gas supply system. These atomizers routinely operate efficiently with sample volumes compatible with the maximum material injection limits of MIPs. An ETA will evaporate the solvent, vaporize the sample, and atomize the analyte, requiring the plasma only to excite the analyte atoms.

Early ETAs used for MIP sample injection consisted of platinum filaments which were inserted into the support gas stream after application and drying of the sample (23, 39). Other versions (117-125) utilized tantalum or tungsten filaments or strips for gaseous analyte production. Although interfacing an ETA to an MIP is mechanically straightforward, tandem operation of the two components has required careful manipulation of the instrumental variables. After application of liquid sample to the ETA filament or strip,

which is usually situated directly in the support gas stream, the rate of solvent evaporation must be carefully controlled. Too great a rate of solvent evaporation can cause the MIP to become unstable or even to extinguish. Valve systems allowing uninterrupted support gas flow and solvent evaporate venting are possible; however, such devices add unnecessary complexity to the system and can result in unstable plasma operation (41). Often, because the walls of the ETA chamber are near ambient temperature, the atomized sample will plate out before transport into the plasma. Proper control of inert gas flow can be used to minimize or eliminate this potential loss mechanism.

Carbon cup and carbon furnace ETAs, which are mechanically less simple to incorporate into an MIP gas system, have also been utilized for sample introduction (126-128). Obviously, these devices cannot be used for the determination of carbon, and also increase the complexity of the plasma background spectrum (41). Such problems can be partially overcome through use of heated metal supports (e.g. Pt boats) (129). Another type of electrothermal atomizer utilizes a high voltage, low current pulsating dc discharge for sample atomization (44, 67). The cathodic sputtering of this microarc atomizer increases the efficiency of analyte atom generation.

6. ANALYTICAL PERFORMANCE AND INTERFERENCES

6.1. Limits of Detection

Table 3 is a compilation of the reported detection limits obtained with argon or helium flowing microwave-induced plasmas. In Table 3, limits of detection are defined as those concentrations which provide a signal magnitude which is a certain multiple of the standard deviation of the

Table 3. Detection Limits for Solution Analysis by Microwave-Induced Plasma

Element	Wavelength(nm)	ng/mL	pg	Reference
Al	309.2	60		45
	396.2	1000		113
Ag	328.1	1-5	1.6-10	67,113,118
As	193.7	30	50-200	45,66,104,120,121,124,126,127
Ba	553.5	100		122,124
B	249.8	10	1.6	45,66,67,127
Be	234.9		100	126
Bi	223.1	0.5	100-200	106,120,126,128
	472.3	1000		113
Cd	228.8	0.4-20	2.8-20	40,45,66,67,106,118
	326.1	40	1	40,121
Ca	39[illegible]	10	10^6	113,130
	422.7	0.16	1.6-10	41,44,67,122
Co	240.7	1-60	10-70	23,45,66,126
	345.4	1000	40	113,118,122
Cr	356.7	1	10	23,127
	425.4	10		45,122
Cu	213.6	100		113
	324.7	0.04-1	0.42-50	23,41,44,45,67,118,120-122
Fe	248.3	1	10	23,45
	372.0	1000	10	23,118,122
Ga	417.2	40		40
Ge	265.2	3	5000	106
Hg	253.7	1-20	0.01-60	38,45,66,67,103,105,121,123,127
Li	670.8		1	67,122
Mg	279.6	500		113,128
	285.2	0.05-1	0.3-0.45	44,45,118,122,128
Mn	279.5	0.05	0.46	44
	403.1	1	0.05-2	44,45,118,121,124
Na	589.0	0.001	0.01	44,67,122
Ni	232.0		100	126
Pb	216.9	1	0.56-2000	44,106
	283.3		0.38-3.8	41,67,130
	405.8	1-100	0.5-300	45,66,106,113,118,120-122,126
Pt	265.9	110	1100	67
Se	196.0	40	100-600	45,66,94,120,126,127
Sb	231.2	100	200-500	113,126,127
Sn	242.9	1000		113
	286.3	2	300-1100	106,120,126
Ti	334.9	100		113
Tl	276.8	0.05	100	106
V	437.9	80		45,66
Zn	213.8	0.04-20	0.35-20	40,44,45,66,67,106,118,120-122,126,130

background noise. The multiple is often one, two, or three, depending on the faith of the original author; we have made no attempt to normalize the values given. Also, ranges of limits of detection are given instead of the lowest value reported. This approach was taken since the range of reported values is a reflection of differences in instrumental application more than a variability in the MIP capability.

Many factors contribute to the limit of detection attainable with an MIP system. The nature of the matrix used, operating pressure, support gas type and flow rate, applied microwave power, and volume of plasma viewed all have their effect. However, of major importance is the selected kind of sample introduction. In general, systems which supply the sample to the MIP in the form of an aerosol exhibit worse detection limits than alternative methods, because of the limited ability of the MIP to evaporate, volatilize, and atomize the droplets and analyte. Desolvation accessories and ultrasonic nebulizers afford improved limits of detection over simpler spray introduction systems. Overall, the best detection limits are obtained with an electrothermal kind of sample atomizer. Although such an atomizer supplies analyte to the MIP in the form of a brief pulse rather than a steady analyte stream, the MIP is allowed to operate more efficiently and thereby provides greater sensitivity.

Future improvements in the detection limits obtainable with MIPs lie in stabilization of the discharge during analyte injection, optimization of the interface between the MIP and ETA in terms of analyte vapor transport time and efficiency, and elimination of the various interferent effects common to MIP systems.

6.2. Interferences

As indicated above, the MIP appears to perform best when it is fed pre-vaporized samples. Accordingly, some interferences which have been reported are ascribable to events in the external atomizer while others actually arise within the MIP itself. In most published work, no attempt has been made to separate these sources of interference, making a meaningful discussion of interference effects difficult. However, it is likely that in many cases, interferences in both atomizer and MIP contribute to the reported effects.

6.2.1. Physical Interferences. The stability and excitation ability of an MIP are perturbed when a sufficient amount of foreign material is injected into it (67). This quenching effect depends somewhat on the nature of the injected atoms, but the property which governs the effect has not been isolated (66, 67). Depending upon the cavity type, sample introduction method, support gas flow rate, operating pressure, and applied power, MIPs can usually withstand the injection of about 1 mg/min (104) or about 3-5μg absolute (44, 67, 130) of foreign material without seriously degrading signal stability. Obviously, such a limitation controls the maximum sample size which can be used with an MIP.

Memory effects have also been reported for the MIP (40, 44), and are probably the result of quartz tube etching by the plasma. Such etching produces a region in the plasma tube in which analyte atoms can collect. The standard remedy is to replace the plasma chamber after a specified number of operating hours.

The presence of refractory elements in a sample matrix sometimes leads to both vaporization and excitation interference problems (6, 45, 66, 67,

113) in an MIP. It is not clear by what mechanism the refractory compounds affect the plasma, possibly by promoting collisional deactivation of metastable species, or creating a competition for these species. The reduction of MIP excitation ability by refractories can often be overcome simply by applying greater microwave power (6, 66). The principal effect of refractory elements on atomizers is to alter the vaporization efficiency or rate of the analyte. For example, Al, Ca, and Pt depress the emission signal of many elements by reducing the rate of analyte volatilization (67, 113). Clearly, the unfavorable effect of refractory elements will be greater for an MIP coupled to a nebulization system than for an MIP fed by an electrothermal atomizer.

The presence of alkali or alkaline earth chlorides in a sample has been shown to enhance the emission signal of other elements in a low-pressure MIP fed by a tantalum strip vaporizer (118, 122, 123, 131). Presumably (122, 131), this enhancement arises from an increase in sample atomization, caused by partial conversion of analyte salts into volatile chlorides. Also, the slope of the log-log analytical calibration curve of some elements is changed to unity (122, 123) when alkalis or alkaline earths are present. Alkali halides possibly affect the excitation conditions within the plasma by introducing competing species into the proposed ionization-radiational excitation mechanisms (122). It is likely that this effect is small compared to the influence of the alkali elements on ionization, discussed below.

6.2.2. "Ionization" Interferences. Ionization interferences can be expected to be significant in an MIP because of its substantial departure from LTE. The importance of electrons to plasma maintenance and analyte excitation (cf. sections 3.2-3.4) would render analyte emission extremely susceptible

to the introduction or depletion of electrons. Although such an influence is beyond that ordinarily termed an "ionization interference", the same kinds of sample-borne species (e.g. alkalis) cause it and the results (i.e. signal enhancement) are the same as described in other analytical sources (6, 45, 56, 113). For example, Na and K have been observed to enhance the emission of Ca (113). The presence of an element of low ionization potential in the MIP is likely to simply result in an increase in the electron density, which will not only affect the plasma, but move the ionization equilibrium of the analyte towards the neutral side (6). This simpler argument has been invoked to explain qualitatively the effects seen (6, 45, 67).

More complex behavior has also been observed. A suppression of Mn emission by alkaline earth elements (132) has been postulated to be caused by bombardment of Mn atoms by the added electrons, causing an enhancement of manganese ionization. Examination of the ionic line emissions from MIPs (130) suggests that those lines will be useful for the determination of some elements, for example Ca, Sr, and Ba. However, it is advised that the determination of elements with low ionization potentials be preceded by an examination of the emission character of both ground state and higher excited state lines.

6.2.3. Addition of Doping Gases. Doping gases (O_2, N_2, H_2) are sometimes added to MIPs serving as GC detectors (42, 79, 85, 95). These dopants usually act as scavengers of hydrocarbon species and carbon deposit eliminators (79, 95). The enhancement effect of doping gases on the analyte emission signal has been suggested to be caused by an increase in the number of species involved in the analyte excitation steps (42). Concentrations of doping gases are usually kept below 2% v/v.

6.2.4. Chemical Interferences. Chemical interferences can arise from several sources, including anions, pH effects, or the formation of stable oxides or other molecular species (45, 67, 113). The emission from Ca in an MIP has been shown to be affected only slightly (113) or not at all (67) by the presence of phosphate while other anionic species have no effect. The formation of stable oxides of the analyte also appears not to be significant for MIPs (67).

6.2.5. Spectral Interferences. Spectral interferences can be a problem with any emission source. Fortunately, argon and helium MIPs have much simpler and less intense background emission spectra than do most flames, arcs, or sparks (44, 67, 130). The continuum background emission in the UV and visible regions is generally low for these gases and can be reduced further through wavelength modulation (53, 66), but it does increase in intensity with pressure (133). The locations of argon and helium spectral lines are well-enough known (58) that those spectral areas may be avoided.

Although matrix elements can contribute to spectral interferences, others can arise from impurities in the support gases (CO_2, water vapor, N_2), from atmospheric species (CO_2, H_2O, N_2), and vaporized elements from the atomization device (usually C, Ta, W, Mo, or Pt) (6, 44). Interference from molecular band and line structure of species such as OH, N_2, H_2, CN, C_2, and NH are common (41, 44), but traps can be used to eliminate most of these support gas impurities (39, 79). Spectral line interference from the element of which the atomizer is composed can be troublesome in choosing analyte lines (67).

References

1. J.D. Cobine and D.A. Wilbur, J. Appl. Phys. 22, 835 (1951).
2. H.P. Broida and M.W. Chapman, Anal. Chem. 30, 2049 (1958).
3. N.S. Ham and A. Walsh, Spectrochim. Acta 8, 12 (1958).
4. W. Schmidt, Elektron. Rundschau 13, 404 (1959).
5. F.E. Lichte, Ph.D. Thesis, Colorado State Univ., 1973.
6. S. Greenfield, H.McL. McGeachin, and P.B. Smith, Talanta 22, 1 (1975).
7. Ibid., 22, 553 (1975).
8. Ibid., 23, 1 (1976).
9. G. Critescu and R. Grigorovici, Bull. Soc. Roum. Phys. 42, 37 (1941).
10. Idem., Opt. Spektrosk. 6, 85 (1959).
11. A.L. Stolov, Uch. Zap. Kazansk. Gos. Univ. 116 (1), 118 (1956).
12. E. Badarau, M.Giurgea, Gh. Giurgea and A.T.H. Trustia, Spectrochim. Acta 11, 441 (1957).
13. H. Dunken, W. Mikkeleit and W. Kniesche, Acta Chim. Acad. Sci. Hung. 33, 67 (1962).
14. M. Yamamoto, Japan J. Appl. Phys. 1, 235 (1962).
15. W. Tappe and J. van Calker, Fresenius' Z. Anal. Chem. 198, 13 (1963).
16. V. Jecht and W. Kessler, Fresenius' Z. Anal. Chem. 198, 27 (1963).
17. R. Mavrodineanu and R.C. Hughes, Spectrochim. Acta 19, 1309 (1963).
18. C.D. West and D.N. Hume, Anal. Chem. 36, 412 (1964).
19. M. Yamamoto and S. Murayama, Spectrochim. Acta 23A, 773 (1967).
20. S. Murayama, H. Matsuno and M. Yamamoto, ibid. 23B, 513 (1968).
21. A.J. McCormack, S.C. Tong and W.D. Cooke, Anal. Chem. 37, 1470 (1965).
22. C.A. Bache and D.J. Lisk, Anal. Chem. 37, 1477 (1965).
23. J.H. Runnels and J.H. Gibson, Anal. Chem. 39, 1398 (1967).

24. B.L. Sharp, Sel. Annu. Rev. Anal. Sci. 4, 37 (1976).

25. A.D. MacDonald, Microwave Breakdown in Gases, John Wiley, New York, N.Y., 1966.

26. S.C. Brown, "Steady Microwave Discharges", ch. 15 in Basic Data of Plasma Physics, MIT Press, Cambridge, MA, 1959.

27. H. Venugopalan, Reactions Under Plasma Conditions, Wiley-Interscience, New York, N.Y., 1971.

28. G. Francis, Ionization Phenomena in Gases, Butterworth, London, 1960, ch. 4.

29. A.D. MacDonald and J.H. Matthews, Can. J. Phys. 34, 395 (1956).

30. P. Leprince, G. Matthieussant, and W.P. Allis, J. Appl. Phys. 42, 412 (1971).

31. R.M. Fredericks and J. Asmussen, J. Appl. Phys. 42, 3647 (1971).

32. R.M. Fredericks and J. Asmussen, Appl. Phys. Lett. 19, 508 (1971).

33. J. Asmussen, R. Mallavarpu, J.R. Hamann, and H.C. Park, Proc. IEEE 62, 109 (1974).

34. J.L. Altman, Microwave Circuits, Van Nostrand, Princeton, N.J., 1964.

35. S.L. Halverson and A.J. Hatch, Appl. Phys. Lett. 14, 79 (1969).

36. K.W. Busch and T.J. Vickers, Spectrochim. Acta 28B, 85 (1973).

37. H.R. Griem, Plasma Spectroscopy, McGraw-Hill, New York, 1964.

38. D.J. Kalnicky, V.A. Fassel, and R.N. Kniseley, Appl. Spectrosc. 31, 137 (1977).

39. H.E. Taylor, J.H. Gibson, and R.K. Skogerboe, Anal. Chem. 42, 1569 (1970).

40. K.R. Fallgatter, V. Svoboda, and J.D. Winefordner, Appl. Spectrosc. 25, 347 (1971).

41. A.T. Zander, R.K. Williams, and G.M. Hieftje, Anal. Chem. 49, 2372 (1977).

42. F.A. Serravallo and T.H. Risby, Anal. Chem. 47, 2141 (1975).

43. P. Brassem and F.J.M.J. Maessen, Spectrochim. Acta 29B, 203 (1974).

44. A.T. Zander and G.M. Hieftje, Anal. Chem. 50, 1257 (1978).

45. R.K. Skogerboe and G.N. Coleman, Anal. Chem. 48, 611A (1976).

46. E.V. Belousov and A.P. Motorenko, Opt. Spektrosk. 30(6), 1006 (1971).

47. E.O. Johnson and L. Malter, Phys. Rev. 80, 58 (1950).

48. R. Avni and J.D. Winefordner, Spectrochim. Acta 30B, 281 (1975).

49. P. Brassem and F.J.M.J. Maessen, Spectrochim. Acta 30B, 547 (1975).

50. P. Brassem, F.J.M.J. Maessen and L.deGalan, Spectrochim. Acta 31B, 537 (1976).

51. J.D. Swift and M.J.R. Schwar, Electrical Probes for Plasma Diagnostics, Elsevier, New York, 1969.

52. C.I.M. Beenakker, Spectrochim. Acta 32B, 173 (1977).

53. P.M. Houpt, Anal. Chim. Acta 86, 129 (1976).

54. C.C. Garber and J.W. Taylor, Anal. Chem. 48, 2070 (1976).

55. F.W. Lampe, T.H. Risby, and F.A. Serravello, Anal. Chem. 49, 560 (1977).

56. A.V. Phelps and J.P. Molnar, Phys. Rev. 89, 1202 (1953).

57. A.R. Striganov, and N.S. Sventitskii, Tables of Spectral Lines of Neutral and Ionized Atoms, IFI/Plenum, New York, 1968.

58. C.E. Moore, An Ultraviolet Multiplet Table, NBS Circular 488, U.S. Government Printing Office, Washington, 1950.

59. C.E. Moore, A Revised Multiplet Table of Astrophysical Interest, NSRDS-NBS 40, U.S. Government Printing Office, Washington, 1972.

60. W.G. Schrenk, S.E. Valente and K.E. Smith, Appl. Spectrosc. 26, 108 (1972).

61. F.C. Fehsenfeld, K.M. Evenson and H.P. Broida, Rev. Sci. Instrum. 36, 294 (1965).

62. S. Ramo, J.R. Whinnery and T. VanDuzer, Fields and Waves in Communications Electronics, John Wiley & Sons, New York, 1965.

63. B. Agdur and B. Eneander, J. Appl. Phys. 33, 575 (1962).

64. P. Rosen, J. Appl. Phys. 20, 868 (1949).

65. R.S. Alger, Electron Paramagnetic Resonance: Techniques and Applications, Interscience, New York, 1968.

66. F.E. Lichte and R.K. Skogerboe, Anal. Chem. 45, 399 (1973).

67. L.R. Layman and G.M. Hieftje, Anal. Chem. 47, 194 (1975).

68. D. Cooke, R.M. Dagnall and T.S. West, Anal. Chim. Acta 56, 17 (1971).

69. G.O. Brink, R.A. Fluegge and R.J. Hull, Rev. Sci. Instrum. 39, 1171 (1968).

70. B. Vidal, and C. Dupret, J. Phys. E. 9, 998 (1976).

71. B. McCarroll, Rev. Sci. Instrum. 41, 279 (1970).

72. T.V. Vorburger, B.J. Waclawski and D.R. Sandstrom, Rev. Sci. Instrum. 47, 501 (1976).

73. C.I.M. Beenakker, Spectrochim. Acta 31B, 483 (1976).

74. C.I.M. Beenakker and P.W.J.M. Boumans, Spectrochim. Acta 33B 53 (1978).

75. S. Hattori, S. Chinen, and H. Ishida, J. Phys E. 4, 280 (1971).

76. L. Bovey, Spectrochim. Acta 10, 432 (1958).

77. J.J. DeCorpo, J.T. Larkins, M.V. McDowell and J.R. Wyatt, Appl. Spectrosc. 29, 85 (1975).

78. J.L. Stanley, H.W. Bentley, and M.B. Denton, Appl. Spectrosc. 27, 265 (1973).

79. J.P.J. vanDalen, P.A. deLezenne-Coulander, and L. deGalan, Anal. Chim. Acta 94, 1 (1977).

80. C. Bache and D. Lisk, Anal. Chem. 38, 1757 (1966).

81. C. Bache and D. Lisk, Anal. Chem. 39, 787 (1967).

82. H.A. Moye, Anal. Chem. 39, 1441 (1967).

83. R.M. Dagnall, S.J. Pratt, T.S. West and D.R. Deans, Talanta 16, 797 (1969).

84. R.M. Dagnall, S.J. Pratt, T.S. West and D.R. Deans, Talanta 17, 1009 (1970).

85. W. Braun, N. Peterson, A. Bass, and M. Kuryko, J. Chrom. 55, 237 (1971).

86. C. Bache and D. Lisk, Anal. Chem. 43, 950 (1971).

87. R.M. Dagnall, T.S. West and P. Whitehead, Anal. Chem. 44, 2074 (1972).

88. R.M. Dagnall, T.S. West and P. Whitehead, Anal. Chim. Acta 60, 25 (1972).

89. W. Grossman, J. Eng and Y.C. Tong, Anal. Chim. Acta 60, 447 (1972).

90. R.M. Dagnall, M. Silvester, T.S. West, and P. Whitehead, Talanta 19, 1226 (1972).

91. D. Natusch and T.M. Thorpe, Anal. Chem. 45, 1185A (1973).

92. R.M. Dagnall, D.J. Johnson and T.S. West, Spectrosc. Lett. 6(2), 87 (1973).

93. H. Kawaguchi, T. Sakamota, and A. Mizuike, Talanta 20, 321 (1973).

94. Y. Talmi and A. Andren, Anal. Chem. 46, 2122 (1974).

95. W.R. McLean, Recent Analytical Developments in the Petroleum Industry, Proc. Inst. Pet. Symp., 1974, Ch. 9.

96. Y. Talmi, Anal. Chim. Acta 74, 107 (1975).

97. Y. Talmi and V.E. Norvell, Anal. Chem. 47, 1510 (1975).

98. Y. Talmi and D. Bostick, Anal. Chem. 47, 2145 (1975).

99. D.C. Reamer, W.H. Zoller, and T.C. O'Haver, Paper #204, Federation of Analytical Chemistry and Spectroscopy Societies, Detroit, MI, 1977.

100. D.T. Bostick and Y. Talmi, J. Chromatogr. Sci. 15, 164 (1977).

101. R.M. Dagnall, T.S. West and P. Whitehead, Analyst (London) 98, 647 (1973).

102. F.A. Serravello and T.H. Risby, Anal. Chem. 48, 673 (1976).

103. F.E. Lichte and R.K. Skogerboe, Anal. Chem. 44, 1480 (1972).

104. F.E. Lichte and R.K. Skogerboe, Anal. Chem. 44, 1321 (1972).

105. R.J. Watling, Anal. Chim. Acta 75, 281 (1975).

106. R.K. Skogerboe, D.L. Dick, D.A. Pavlica, and F.E. Lichte, Anal. Chem. 47, 568 (1975).

107. H.E. Taylor, J.H. Gibson, and R.K. Skogerboe, Anal. Chem 42, 876 (1970).

108. A. van Sandwijk, P.F.E. van Montfort, and J. Agterdenbos, Talanta 20, 495 (1973).

109. A. van Sandwijk and J. Agterdenbos, Talanta 21, 360 (1974).

110. P.F.E. van Montfort and J. Agterdenbos, Talanta 21, 660 (1974).

111. A. van Sandwijk, Chem. Weekbl. 70(38), L11 (1974).

112. R.N. Kniseley, H. Amenson, C.C. Butler and V.A. Fassel, Appl. Spectrosc. 28, 285 (1974).

113. H. Kawaguchi, M. Hasegawa, and A. Mizuike, Spectrochim. Acta 27B, 205 (1972).

114. H. Kawaguchi, M. Okada and A. Mizuike, Bunseki Kagaku 25, 344 (1976).

115. W. Kessler, Glastech. Ber. 44, 479 (1971).

116. K. Govindaraju, G. Mevelle, and C. Chouard, Anal. Chem. 48, 1325 (1976).

117. K.M. Aldous, R.M. Dagnall, B.L. Sharp, and T.S. West, Anal. Chim. Acta 54, 233 (1971).

118. H. Kawaguchi and B. Vallee, Anal. Chem. 47, 1029 (1975).

119. H. Kawaguchi and D. Auld, Clin. Chem. 21, 591 (1975).

120. F.L. Fricke, O. Rose, and J.A. Caruso, Talanta 23, 317 (1976).

121. G.F. Kirkbright, Paper #454, Pittsburgh Conference on Analytical Chemistry and Applied Spectroscopy, Cleveland, Ohio, March, 1977.

122. H. Kawaguchi, I. Atsuya, and B.L. Vallee, Anal. Chem. 49, 266 (1977).

123. I. Atsuya, H. Kawaguchi and B.L. Vallee, Anal. Biochem. 77, 208 (1977).

124. I. Atsuya, G.M. Alter, C. Veillon, and B.L. Vallee, Anal. Biochem. 79, 202 (1977).

125. T. Sakamoto, H. Kawaguchi and A. Mizuike, Bunko Kenkyu 25, 35 (1976).

126. F.L. Fricke, O. Rose and J.A. Caruso, Anal. Chem. 47, 2018 (1975).

127. G. Kaiser, D. Götz, P. Schoch and G. Tölg, Talanta 22, 889 (1975).

128. O. Rose, D.W. Mincey, A.M. Yacynych, W.R. Heineman, and J.A. Caruso, Analyst 101, 753 (1976).

129. D.G. Mitchell, K.M. Aldous and E. Canelli, Anal. Chem. 49, 1235 (1977).

130. A.T. Zander, R.K. Williams and G.M. Hieftje, paper no. 72, Federation of Analytical Chemistry and Spectroscopy Societies, Detroit, MI., 1977.

131. I. Atsuya, H. Kawaguchi, C. Veillon and B.L. Vallee, Anal. Chem. 49. 1489 (1977).

132. K. Kitagawa and T. Takeuchi, Anal. Chim. Acta 67, 453 (1973).

133. J.P. Campbell, E.W. Spisz and R.L. Bowman, Appl. Opt. 10, 2555 (1971).

ACKNOWLEDGEMENT

Preparation of this review was supported in part by the Office of Naval Research and by the National Science Foundation.

FIGURE CAPTIONS

Figure 1 Theoretical power-loss and power-absorbed curves in a plasma of constant excitation temperature and background pressure (see text for discussion).

A. Power-loss curve

B. Power-absorbed curve: applied power is $P_a(1)$, cavity length is L_1.

C. Power-absorbed curve: applied power is $P_a(2)$ which is greater than $P_a(1)$: cavity length is L_1.

D. Power-absorbed curve: applied power is $P_a(2)$, cavity length is L_2.

Stability implied at points 1, 4, 5, and 6.

Instability implied at points 2 and 3.

(Adapted from reference 30.)

Figure 2a Tapered Rectangular, TE_{013} Mode Cavity

2b Foreshortened 3/4-wave Coaxial Cavity

2c Foreshortened 3/4-wave Coaxial Cavity, with impedance matching stub located on the coaxial connector.

2d Foreshortened 1/4-wave Coaxial Cavity.

2e Foreshortened 1/4-wave Radial Cavity.

Figure 3 TM_{010} Mode Cavity

1. Cavity wall
2. Fixed bottom
3. Removable cover
4. Plasma chamber (quartz tube)
5. Chamber mount
6. Copper wire coupling loop
7. UG-58 RF connector
8. Ceramic insulator
9. Tuning stub
10. Tuning stub
11. Port for viewing or input of coolant gas
12. Optical bench mount

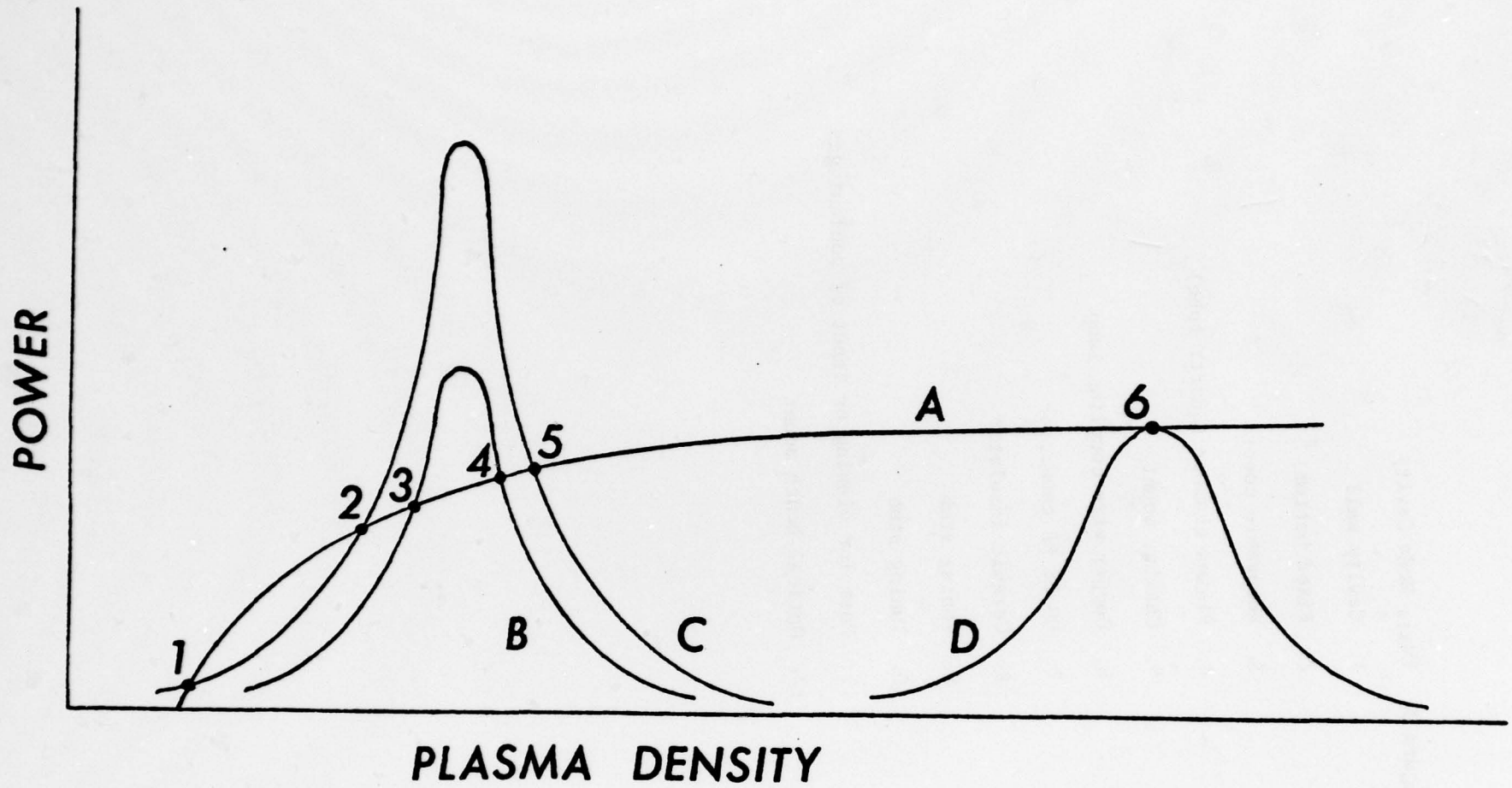
POWER
PLASMA DENSITY
A
B
C
D
1
2
3
4
5
6

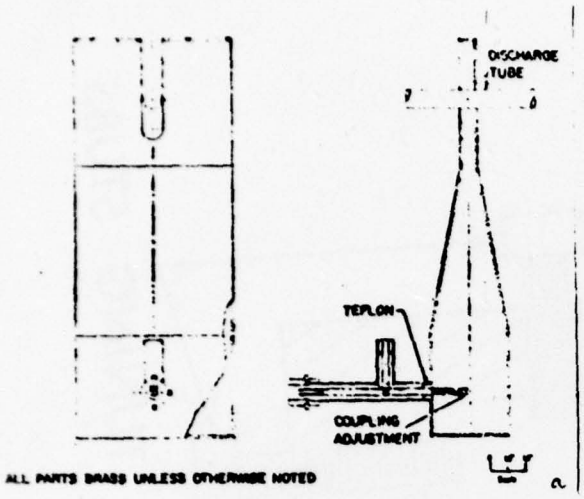
DISCHARGE TUBE
TEFLON
COUPLING ADJUSTMENT
ALL PARTS BRASS UNLESS OTHERWISE NOTED
a

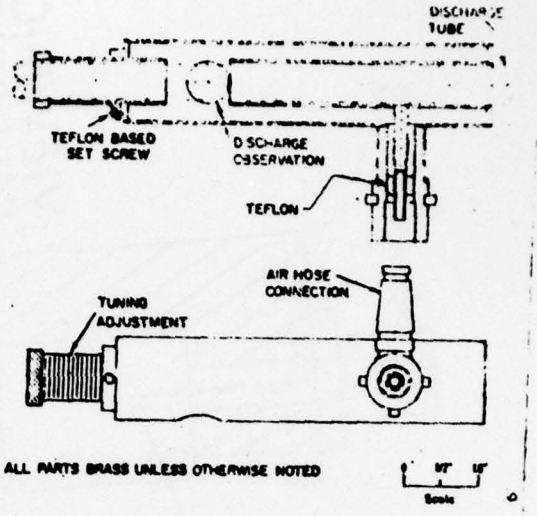
DISCHARGE TUBE
TEFLON BASED SET SCREW
DISCHARGE OBSERVATION
TEFLON
AIR HOSE CONNECTION
TUNING ADJUSTMENT
ALL PARTS BRASS UNLESS OTHERWISE NOTED
Scale
b

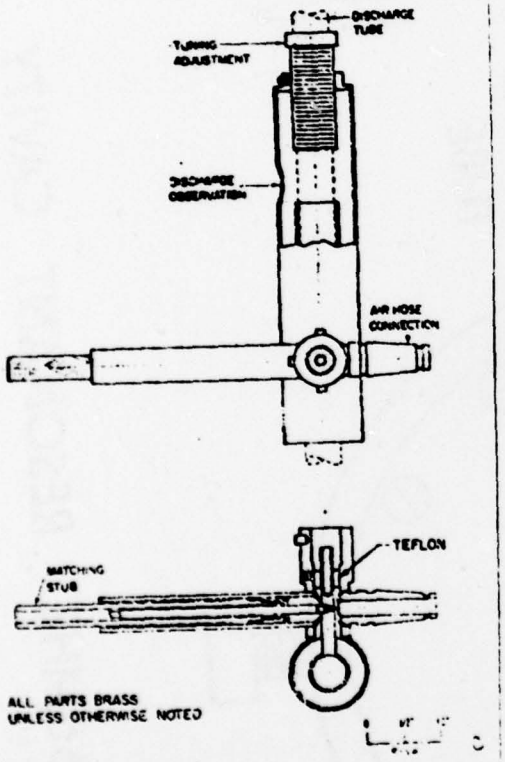
DISCHARGE TUBE
TUNING ADJUSTMENT
DISCHARGE OBSERVATION
AIR HOSE CONNECTION
TEFLON
MATCHING STUB
ALL PARTS BRASS UNLESS OTHERWISE NOTED
c

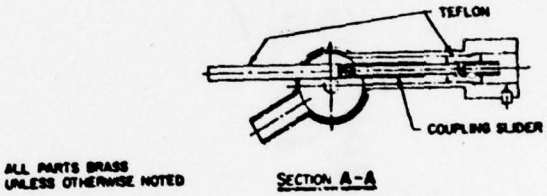
TEFLON
COUPLING SLIDER
ALL PARTS BRASS UNLESS OTHERWISE NOTED
SECTION A-A

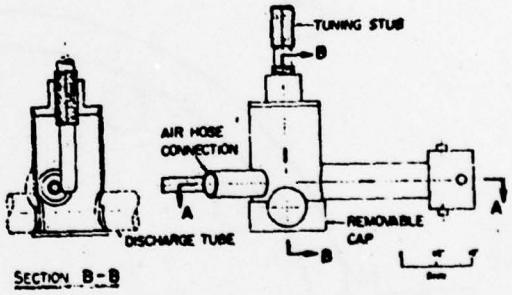
TUNING STUB
B
AIR HOSE CONNECTION
A
A
REMOVABLE CAP
DISCHARGE TUBE
B
SECTION B-B
d

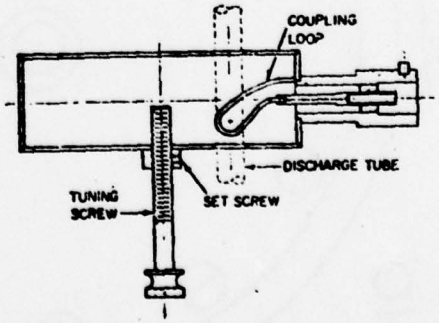
COUPLING LOOP
DISCHARGE TUBE
TUNING SCREW
SET SCREW

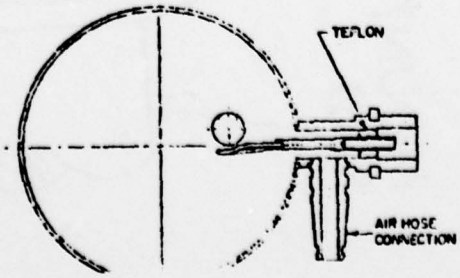
TEFLON
AIR HOSE CONNECTION

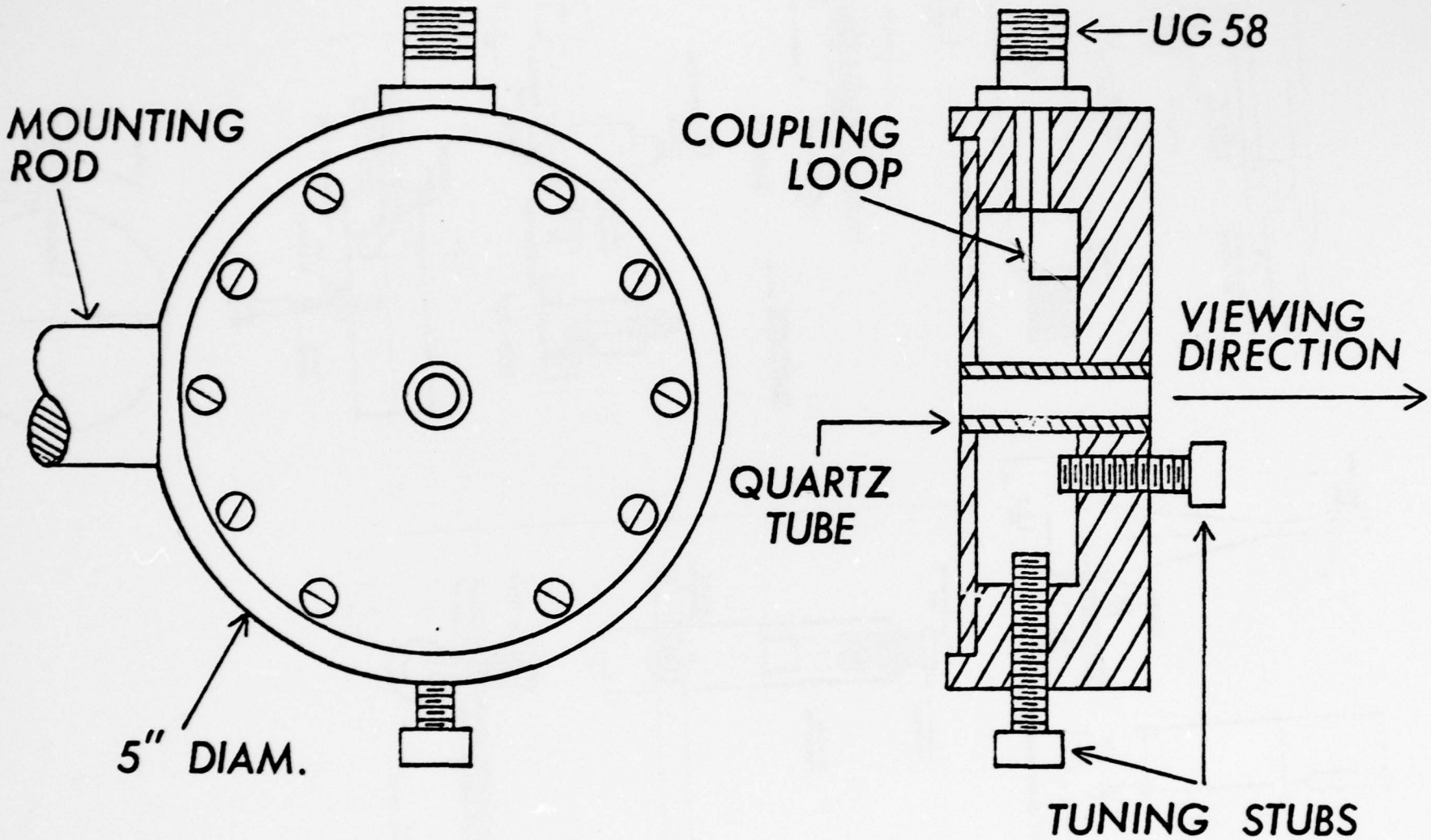

2450MHZ RESONANT CAVITY

472:GAN:716:tam
78u472-608

TECHNICAL REPORT DISTRIBUTION LIST, GEN

	No. Copies
Office of Naval Research 800 North Quincy Street Arlington, Virginia 22217 Attn: Code 472	2
ONR Branch Office 536 S. Clark Street Chicago, Illinois 60605 Attn: Dr. George Sandoz	1
ONR Branch Office 715 Broadway New York, New York 10003 Attn: Scientific Dept.	1
ONR Branch Office 1030 East Green Street Pasadena, California 91106 Attn: Dr. R. J. Marcus	1
ONR Area Office One Hallidie Plaza, Suite 601 San Francisco, California 94102 Attn: Dr. P. A. Miller	1
ONR Branch Office Building 114, Section D 666 Summer Street Boston, Massachusetts 02210 Attn: Dr. L. H. Peebles	1
Director, Naval Research Laboratory Washington, D.C. 20390 Attn: Code 6100	1
The Assistant Secretary of the Navy (R,E&S) Department of the Navy Room 4E736, Pentagon Washington, D.C. 20350	1
Commander, Naval Air Systems Command Department of the Navy Washington, D.C. 20360 Attn: Code 310C (H. Rosenwasser)	1
Defense Documentation Center Building 5, Cameron Station Alexandria, Virginia 22314	12
U.S. Army Research Office P.O. Box 1211 Research Triangle Park, N.C. 27709 Attn: CRD-AA-IP	1
Naval Ocean Systems Center San Diego, California 92152 Attn: Mr. Joe McCartney	1
Naval Weapons Center China Lake, California 93555 Attn: Dr. A. B. Amster Chemistry Division	1
Naval Civil Engineering Laboratory Port Hueneme, California 93401 Attn: Dr. R. W. Drisko	1
Professor K. E. Woehler Department of Physics & Chemistry Naval Postgraduate School Monterey, California 93940	1
Dr. A. L. Slafkosky Scientific Advisor Commandant of the Marine Corps (Code RD-1) Washington, D.C. 20380	1
Office of Naval Research 800 N. Quincy Street Arlington, Virginia 22217 Attn: Dr. Richard S. Miller	1
Naval Ship Research and Development Center Annapolis, Maryland 21401 Attn: Dr. G. Bosmajian Applied Chemistry Division	1
Naval Ocean Systems Center San Diego, California 91232 Attn: Dr. S. Yamamoto, Marine Sciences Division	

Encl 1

472:GAN:716:tam
78u472-608

TECHNICAL REPORT DISTRIBUTION LIST, 051C

	No. Copies
Dr. M. B. Denton University of Arizona Department of Chemistry Tucson, Arizona 85721	1
Dr. R. A. Osteryoung Colorado State University Department of Chemistry Fort Collins, Colorado 80521	1
Dr. B. R. Kowalski University of Washington Department of Chemistry Seattle, Washington 98105	1
Dr. S. P. Perone Purdue University Department of Chemistry Lafayette, Indiana 47907	1
Dr. D. L. Venezky Naval Research Laboratory Code 6130 Washington, D.C. 20375	1
Dr. H. Freiser University of Arizona Department of Chemistry Tuscon, Arizona 85721	
Dr. Fred Saalfeld Naval Research Laboratory Code 6110 Washington, D.C. 20375	1
Dr. H. Chernoff Massachusetts Institute of Technology Department of Mathematics Cambridge, Massachusetts 02139	1

	No. Copies
Dr. K. Wilson University of California, San Diego Department of Chemistry La Jolla, California 92037	1
Dr. A. Zirino Naval Undersea Center San Diego, California 92132	1
Dr. John Duffin United States Naval Postgraduate School Monterey, California 93940	1
Dr. G. M. Hieftje Department of Chemistry Indiana University Bloomington, Indiana 47401	1
Dr. Victor L. Rehn Naval Weapons Center Code 3813 China Lake, California 93555	1
Dr. Christie G. Enke Michigan State University Department of Chemistry East Lansing, Michigan 48824	1
Dr. Kent Eisentraut, MBT Air Force Materials Laboratory Wright-Patterson AFB, Ohio 45433	1
Walter G. Cox, Code 3632 Naval Underwater Systems Center Building 148 Newport, Rhode Island 02840	1